Journal of the European Ceramic Society 40 (2020) 3592–3599

Contents lists available at ScienceDirect

Journal of the European Ceramic Society

journal homepage: www.elsevier.com/locate/jeurceramsoc

Original Article

Enhanced thermal stability of Bi_2Te_3-based alloys via interface engineering with atomic layer deposition

Sang-Soon Lim[a,b], Kwang-Chon Kim[a], Hansol Jeon[c], Ju-Young Kim[c], Jun-Yun Kang[d], Hyung-Ho Park[b], Seung-Hyub Baek[a,b,e,f], Jin-Sang Kim[a,*], Seong Keun Kim[a,*]

[a] Center for Electronic Materials, Korea Institute of Science and Technology, Seoul 02792, Republic of Korea
[b] Department of Materials Science and Engineering, Yonsei University, Seoul 03722, Republic of Korea
[c] School of Materials Science and Engineering, Ulsan National Institute of Science and Technology (UNIST), Ulsan 44919, Republic of Korea
[d] Ferrous Alloy Department, Korea Institute of Materials Science, Changwon 51508, Republic of Korea
[e] Yonsei-KIST Convergence Research Institute, Seoul 02792, Republic of Korea
[f] Division of Nano & Information Technology, KIST School, Korea University of Science and Technology, Seoul 02792, Republic of Korea

ARTICLE INFO

Keywords:
Thermal stability
Bi_2Te_3
Atomic layer deposition
Heterogeneous interfaces
Te sublimation

ABSTRACT

The ease of Te sublimation from Bi_2Te_3-based alloys significantly deteriorates thermoelectric and mechanical properties via the formation of voids. We propose a novel strategy based on atomic layer deposition (ALD) to improve the thermal stability of Bi_2Te_3-based alloys via the encapsulation of grains with a ZnO layer. Only a few cycles of ZnO ALD over the $Bi_2Te_{2.7}Se_{0.3}$ powders resulted in significant suppression of the generation of pores in $Bi_2Te_{2.7}Se_{0.3}$ extrudates and increased the density even after post-annealing at 500 °C. This is attributed to the suppression of Te sublimation from the extrudates. The ALD coating also enhanced grain refinement in $Bi_2Te_{2.7}Se_{0.3}$ extrudates. Consequently, their mechanical properties were significantly improved by the encapsulation approach. Furthermore, the ALD approach yields a substantial improvement in the figure-of-merit after the post-annealing. Therefore, we believe the proposed approach using ALD will be useful for enhancing the mechanical properties of Bi_2Te_3-based alloys without sacrificing thermoelectric performance.

1. Introduction

Thermoelectric devices have attracted significant interest for numerous applications ranging from sustainable energy harvesting from waste heat to solid-state coolers [1,2]. The performance of thermoelectric devices is largely determined by the figure-of-merit (ZT) of thermoelectric materials. $ZT = S^2\sigma T/\kappa$, where S is the Seebeck coefficient, σ is the electrical conductivity, T is the absolute temperature, and κ is the thermal conductivity. These thermoelectric parameters are strongly coupled with each other. Significant efforts have been devoted to the enhancement of ZT values based on the optimisation of thermoelectric parameters [3–6]. Bi_2Te_3-based alloys are the only thermoelectric materials that are commercially available because these alloys have the highest ZT values near room temperature.

In addition to the enhancement of thermoelectric performance, excellent mechanical properties of thermoelectric materials are required for many practical applications. Thermoelectric materials are typically exposed to various mechanical stimuli (e.g., clamping forces, mechanical stresses generated by large thermal gradients, and environmental vibration) during module fabrication and in practical use. These external stresses may result in the critical failure of thermoelectric devices. Bi_2Te_3-based materials are composed of quintuple layers bonded by weak van der Waals interactions. Therefore, cracks can easily propagate along the basal plane, leading to significant mechanical failures, even with relatively weak external stimuli. Several approaches, including grain refinement and the precipitation of heterogeneous materials in the matrix, have been proposed to improve the mechanical properties of Bi_2Te_3-based alloys [7–9]. These approaches generate many interfaces that can halt crack propagation, thereby improving the hardness of Bi_2Te_3-based alloys.

Materials formed at low processing temperatures include many defects, such as dislocations, micropores, and vacancies. These defects can deteriorate the thermoelectric and mechanical properties of thermoelectric materials. However, high-temperature processing can cause Te sublimation from Bi_2Te_3-based alloys [10,11]. Te sublimation adversely affects both electrical and mechanical properties. First, electronic carrier density is modified by the generation of point defects, such as tellurium vacancies ($V_{Te}^{\cdot\cdot}$), and antisite defects (Sb_{Te}' and Bi_{Te}').

* Corresponding authors.
E-mail addresses: jskim@kist.re.kr (J.-S. Kim), s.k.kim@kist.re.kr (S.K. Kim).

https://doi.org/10.1016/j.jeurceramsoc.2020.04.013
Received 30 January 2020; Received in revised form 6 April 2020; Accepted 7 April 2020
Available online 15 April 2020
0955-2219/

Second, porosity can be generated during high-temperature processing, leading to a reduction in the mechanical strength of Bi_2Te_3-based alloys. Therefore, it is crucial to develop an innovative method of suppressing the sublimation of Te while obtaining high-quality Bi_2Te_3-based alloys via high-temperature processing.

The surface coating of thermoelectric legs with high-temperature polymers [12,13] and Si_3N_4 layers [14] has been proposed to prevent sublimation and oxidation. Given that the sublimation of Te occurs mainly along the grain boundaries of Bi_2Te_3-based alloys [15], the encapsulation of grains with a protective layer would be an effective strategy for suppressing the sublimation of Te during high-temperature processing. Atomic layer deposition (ALD) is promising method that can achieve the conformal encapsulation of grains based on its self-limiting growth mechanism. We reported the successful synthesis of thermoelectric materials designed with $Bi_{0.4}Sb_{1.6}Te_3$-ZnO core-shell structures via the ALD technique [16]. Additionally, ALD facilitates grain refinement after high-temperature processing [16], which could be useful for hardening Bi_2Te_3-based alloys.

In this study, we fabricated the n-type thermoelectric material $Bi_2Te_{2.7}Se_{0.3}$ with abundant heterointerfaces based on the introduction of ZnO thin layers via ALD. ZnO layers were selected as the protecting layers for $Bi_2Te_{2.7}Se_{0.3}$ grains because ZnO is thermally stable (melting point of 1975 °C) and has low volatility. ZnO-coated $Bi_2Te_{2.7}Se_{0.3}$ powders were sintered via hot extrusion and subsequently annealed at 500 °C, as shown in Fig. 1. The thermal stability and mechanical properties of the extrudates were analysed in terms of ZnO ALD cycles. The drastic suppression of Te sublimation was achieved via the ALD of very thin ZnO layers. The enhancement of mechanical properties was also achieved based on the microstructural design of grain encapsulation. The thermoelectric properties of the extrudates were also analysed.

2. Experimental procedure

2.1. Material preparation

Bi (99.999 %), Te (99.999 %), and Se (99.999 %) granules were used as starting materials. The materials were weighed to achieve a composition of $Bi_2Te_{2.7}Se_{0.3}$. After vacuum sealing (approximately 10^{-5} Torr) in a quartz tube, the materials were melted in a rocking furnace at 800 °C for 6 h, followed by water quenching. The resulting $Bi_2Te_{2.7}Se_{0.3}$ chunks were ball-milled with zirconia balls under an Ar atmosphere. The weight ratio of the balls and materials was fixed at 3:1 and the grinding process was conducted at 1200 rpm for 24 h.

ZnO thin films were grown on $Bi_2Te_{2.7}Se_{0.3}$ powders contained in a vibrating chamber via ALD at room temperature. Diethylzinc (DEZ) and H_2O were used as Zn and O sources, respectively. One ZnO ALD cycle consisted of DEZ feeding (20 min) – purging (30 min) – H_2O feeding (20 min) – purging (30 min). The thickness of the ZnO films on the $Bi_2Te_{2.7}Se_{0.3}$ powders was varied by the changing the number of ALD cycles.

A green body was prepared by cold-pressing the ZnO-coated $Bi_2Te_{2.7}Se_{0.3}$ powders. Hot extrusion was then performed at 460 °C under a uniaxial pressure of 50 MPa. The resulting extrudate had a diameter of 3 mm. The extrudate was subsequently annealed in a vacuum-sealed quartz tube (approximately 10^{-5} Torr) at 500 °C for 30 h.

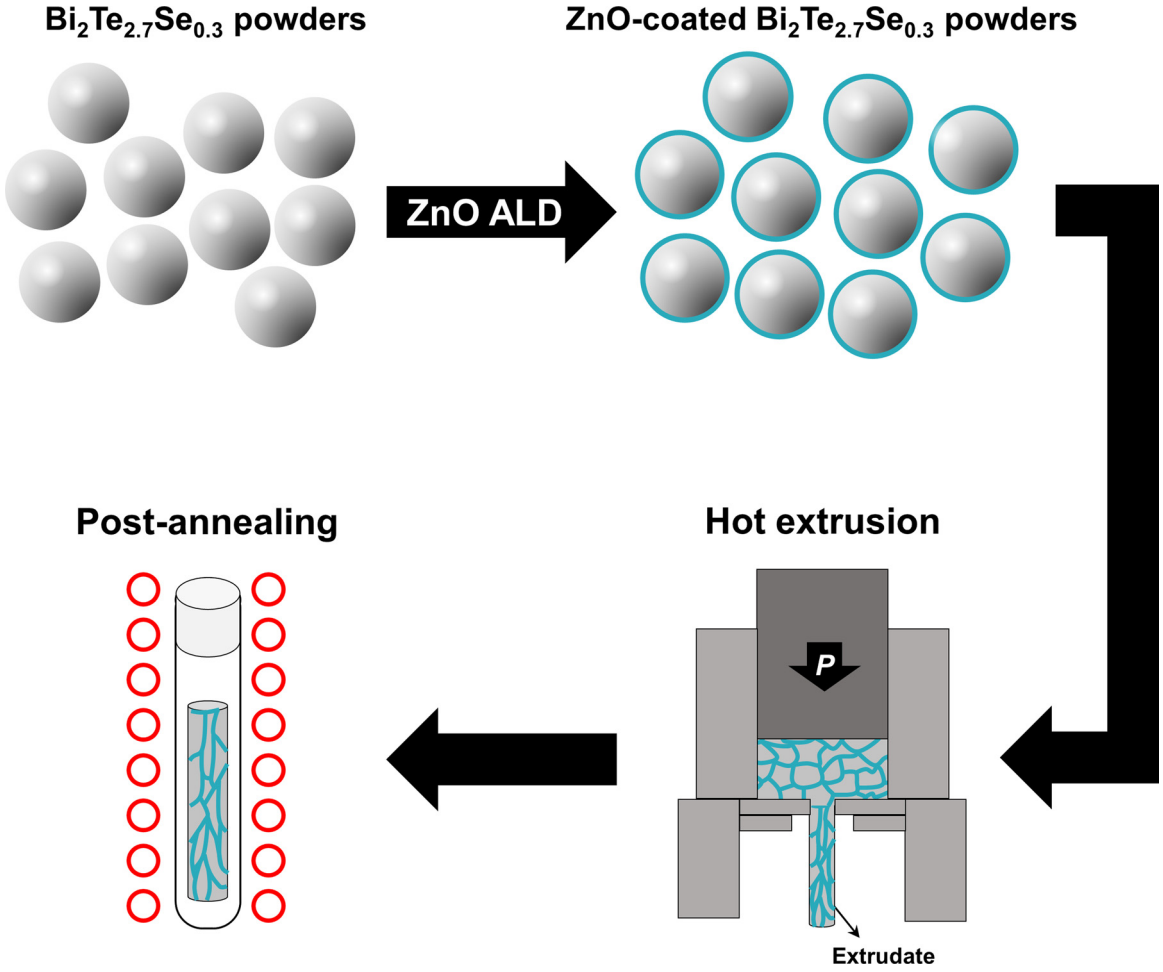

Fig. 1. Schematic process diagram for the synthesis of ZnO-coated $Bi_2Te_{2.7}Se_{0.3}$ extrudates.

2.2. Material characterisation & measurement

The volume of the samples was estimated using the Archimedes' method. The microstructures of the samples were analysed using scanning electron microscopy (SEM, S-4300, Hitachi) and transmission electron microscopy (TEM, Talos F200X, FEI). The Seebeck coefficient was measured using a method based on the slope of a voltage versus temperature-gradient curve. Electrical conductivity was measured using a conventional four probe method with an AC power source. Hall measurement was performed to evaluate the carrier density and mobility of the samples. A Van de Pauw geometry was used for the Hall measurement at a direct current of 18 mA and a magnetic field of 0.55 T. ZT values were calculated using the Harman method, which excludes parasitic effects [17,18]. The thermal conductivity was estimated using $\kappa = S^2/\sigma Z$. All the thermoelectric properties were measured along a direction parallel to the extrusion direction. A nanoindentation testing (Nano Indenter G200, KLA) was used to measure the mechanical properties of the samples. Thermal stability was analysed via thermogravimetric analysis (TGA, Q600, TA instrument) up to 600 °C with a ramping speed of 6 °C/min.

3. Results & discussion

Prior to investigating the effects of ZnO ALD on $Bi_2Te_{2.7}Se_{0.3}$, it was necessary to confirm the presence of dispersed ZnO/$Bi_2Te_{2.7}Se_{0.3}$ heterogeneous interfaces in the extruded samples. It was previously reported that the ALD process readily forms a core-shell structure of ZnO-enclosed Bi_2Te_3 particles, even with extremely small powders (≤20 nm), and many ZnO/Bi_2Te_3 heterogeneous grain boundaries were eventually created in spark plasma sintered samples [16]. However, the sintering of materials during the hot extrusion is different from that during spark plasma sintering. Hot extrusion severely deforms green bodies under unidirectional pressure. Because $Bi_2Te_{2.7}Se_{0.3}$ is a layer-structured material with weak van der Waals interactions, its grains are split and the basal plane of the grains is aligned parallel to the extrusion direction [19,20]. Therefore, the heterogeneous ZnO/$Bi_2Te_{2.7}Se_{0.3}$ interfaces can be destroyed by the grain reconstruction that occurs during the hot extrusion process.

TEM analysis was performed to examine the microstructures of extrudates. Fig. 2 (a) presents a high-angle annular dark-field scanning TEM image of a 7-cycle-ZnO-coated $Bi_2Te_{2.7}Se_{0.3}$ extrudate annealed at 500 °C. The TEM energy-dispersive spectroscopy (EDS) element maps corresponding to the area observed in Fig. 2 (a) are also presented in Figs. S1 (a)–(e) for elements of (a) Zn, (b) O, (c) Bi, (d) Te, and (e) Se, respectively. Despite hot extrusion and post-annealing at a high temperature, the $Bi_2Te_{2.7}Se_{0.3}$ fine grains (diameter ≤ 3 μm) are enclosed by the ZnO layer. The heterogeneous ZnO/$Bi_2Te_{2.7}Se_{0.3}$ interfaces are well developed in the annealed extrudate. Given that the signal intensities of Zn and O do not overlap with those of Bi, Te, and Se in the EDS element maps in Figs. S1 (a)–(e), we can conclude that severe intermixing of elements did not occur. Additionally, the heterogeneous interfaces were found to be loosely aligned along the extrusion direction. This indicates that hot extrusion facilitates the texturing of microstructure, even in the ZnO-coated $Bi_2Te_{2.7}Se_{0.3}$.

In addition to local microstructure observations using TEM, it is necessary to identify the phase purity of the materials following ZnO coating and post-annealing at high temperatures on a mesoscopic scale. Fig. 2 (b) presents X-ray diffraction (XRD) patterns of uncoated $Bi_2Te_{2.7}Se_{0.3}$ and 1-, 5-, 7-, and 10-cycle-ZnO-coated $Bi_2Te_{2.7}Se_{0.3}$ extrudates following post-annealing at 500 °C. The extrudates were positioned to detect crystal planes parallel to the extrusion direction during XRD analysis based on their anisotropic microstructures. All of the diffraction peaks shown in Fig. 2 (b) correspond to the Bragg peaks of rhombohedral $Bi_2Te_{2.7}Se_{0.3}$, regardless of the number of ZnO ALD cycles. Peaks corresponding to off-stoichiometric bismuth telluride alloys, such as Bi_3Te_4 and Bi_4Te_5, are not observed, even after post-annealing at 500 °C. The Bragg peaks of ZnO are also undetectable for up to 10 cycles of ZnO ALD, which can be attributed to the relatively small mass fraction of the ZnO layer. These results suggest that ALD coating does not induce significant changes in the crystal phase of extrudates. Therefore, heterogeneous ZnO/$Bi_2Te_{2.7}Se_{0.3}$ interfaces are expected to be uniformly distributed throughout post-annealed extrudates.

Annealing is a promising method for improving the thermoelectric performance of Bi_2Te_3-based alloys [10,21]. Bi_2Te_3-based alloys typically have various types of defects, such as antisite defects, vacancies, and dislocations. These defects are often inhomogeneously distributed in sintered alloys. These defects and their inhomogeneity can significantly deteriorate the thermoelectric properties of materials. It has

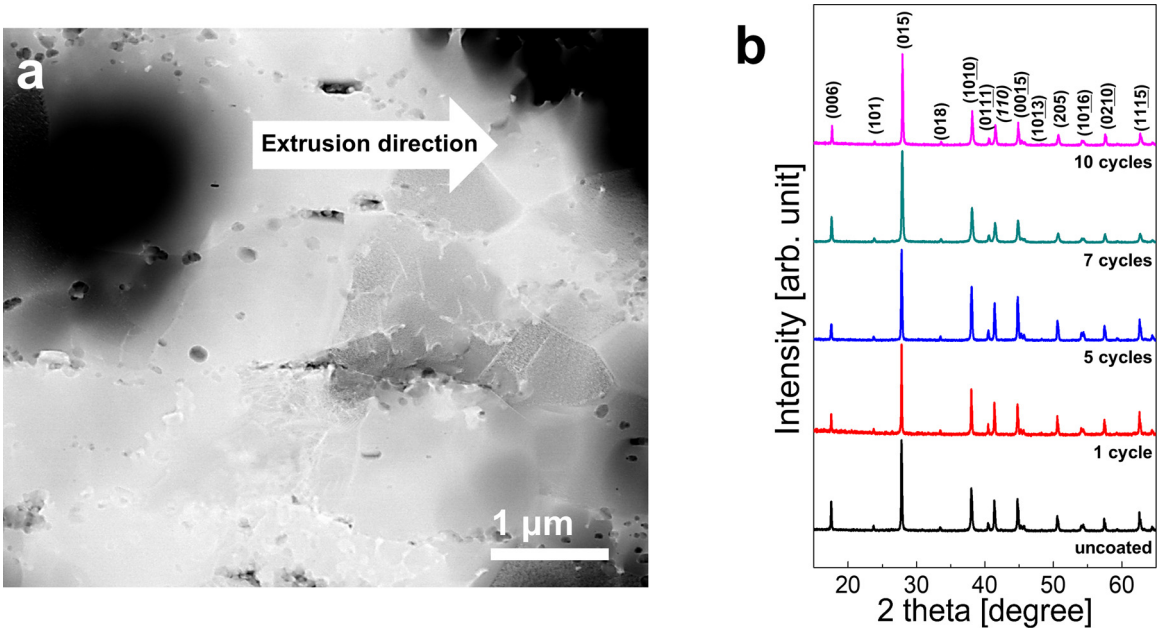

Fig. 2. (a) High-angle annular dark-field scanning TEM image of a 7-cycle-ZnO-coated $Bi_2Te_{2.7}Se_{0.3}$ extrudate annealed at 500 °C. (b) θ-2θ XRD patterns of uncoated $Bi_2Te_{2.7}Se_{0.3}$ and 1-, 5-, 7-, and 10-cycle-ZnO-coated $Bi_2Te_{2.7}Se_{0.3}$ extrudates following post-annealing at 500 °C. The detected crystal planes are parallel to the extrusion direction.

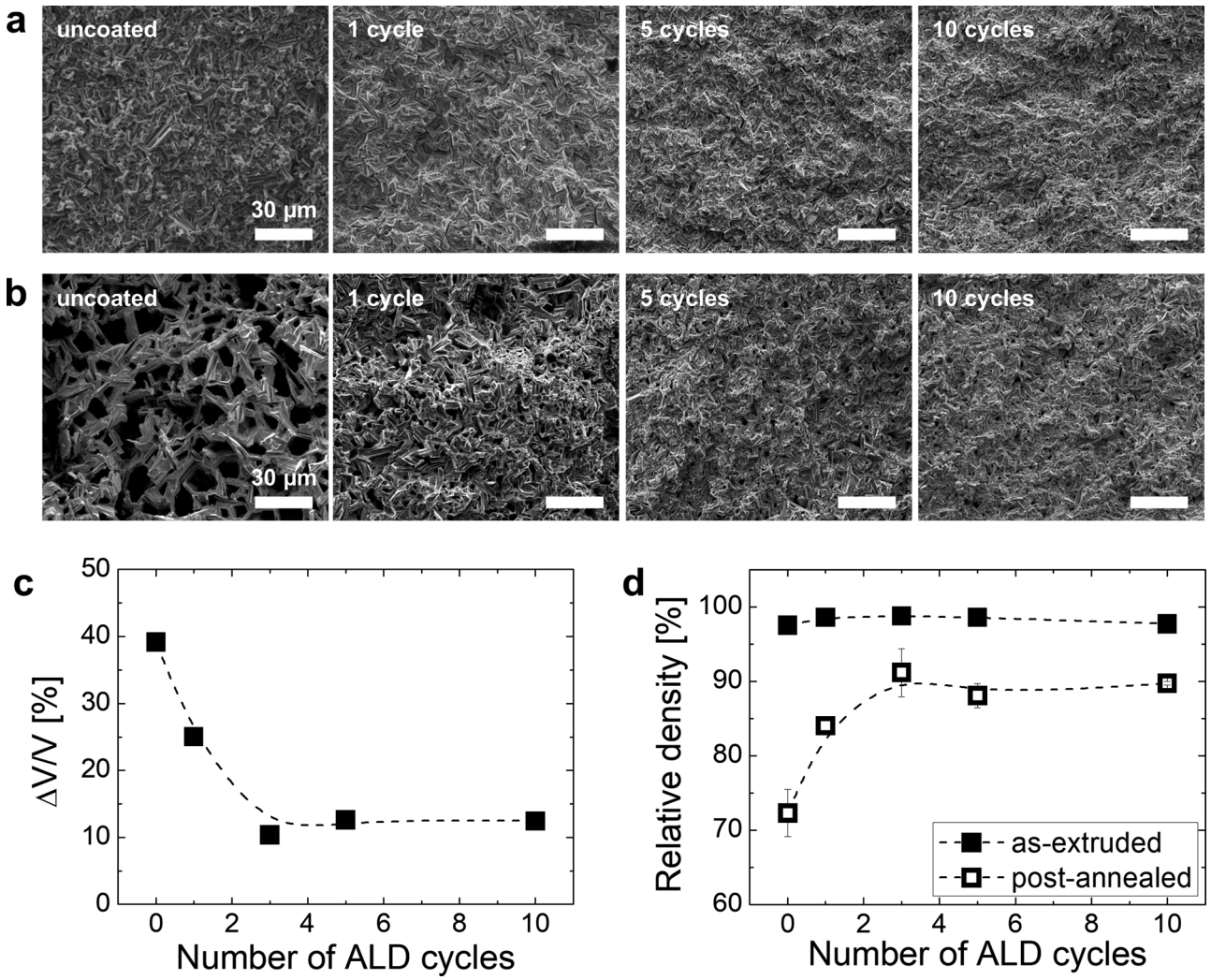

Fig. 3. SEM images of the fracture surfaces of (a) as-extruded and (b) post-annealed samples with 0, 1, 5, and 10 ZnO ALD cycles. Variations in the (c) volume expansion and (d) relative density of extrudates as a function of the number of ZnO ALD cycles.

been extensively reported that post-annealing following sintering can reduce defects and alleviate inhomogeneity [22,23]. However, annealing may also induce adverse microstructural effects [24], resulting in the degradation of mechanical properties [25].

Therefore, it is necessary to examine changes in the microstructures of ZnO-coated $Bi_2Te_{2.7}Se_{0.3}$ extrudates following post-annealing. Figs. 3 (a) and (b) present SEM images of the fracture surfaces of uncoated $Bi_2Te_{2.7}Se_{0.3}$ and 1-, 5-, and 10-cycle-ZnO-coated $Bi_2Te_{2.7}Se_{0.3}$ extrudates (a) before and (b) after post-annealing at 500 ˚C for 30 h. The fracture surfaces perpendicular to the extrusion direction are compared in Fig. 3 (a) and (b). Although all of the as-extruded materials exhibit dense fracture surfaces, regardless of the number of cycles of ZnO ALD, the ALD coating of ZnO results in significant differences in the evolution of microstructures following post-annealing. After post-annealing, many large pores appear for the uncoated $Bi_2Te_{2.7}Se_{0.3}$, while the formation of pores is considerably suppressed by a single cycle of ZnO ALD. Very few pores can be observed above three cycles of ZnO ALD. For a quantitative comparison, changes in the volume and density of the extrudates with post-annealing were analysed in terms of the number of cycles of ZnO ALD (Fig. 3 (c) and (d)). The volume of the uncoated $Bi_2Te_{2.7}Se_{0.3}$ increases by approximately 40 % following post-annealing because of the presence of pores generated by Te sublimation. It has been reported that Te easily sublimates from Bi_2Te_3-based alloys at high temperatures [10,11]. Additionally, Te sublimation involves a decrease in the density of Bi_2Te_3-based alloys. The uncoated $Bi_2Te_{2.7}Se_{0.3}$ extrudate has relatively low density at approximately 70 % of the theoretical density (7.86 g/cm^3) [26] of $Bi_2Te_{2.7}Se_{0.3}$. In contrast, the volume expansion of the ZnO-coated $Bi_2Te_{2.7}Se_{0.3}$ is significantly reduced by the incorporation of the ALD ZnO layer. Volume expansion is reduced to as little as 10 % over three ALD cycles of ZnO. The effective suppression of volume expansion leads to an increase in the density of the extrudates containing ZnO to approximately 90 % of the theoretical value.

To gain a deeper understanding of the role of the ALD ZnO layers in the extrudates, differences in the weight loss of the extrudates at high temperatures were analysed with and without ZnO ALD. Fig. 4 shows the TGA data of 0, 1, 5, 7, and 10-cycle-ZnO-coated $Bi_2Te_{2.7}Se_{0.3}$. The TGA data in Fig. 4 reveal that the weight loss of the ZnO-coated $Bi_2Te_{2.7}Se_{0.3}$ samples is smaller than that of the uncoated $Bi_2Te_{2.7}Se_{0.3}$ at high temperatures. This indicates that the introduction of ZnO directly suppresses the sublimation of Te from $Bi_2Te_{2.7}Se_{0.3}$, which is closely related to a microstructure in which $Bi_2Te_{2.7}Se_{0.3}$ grains are encapsulated by very thin ZnO layers (Fig. 2). Although the tendency of the change in the weight loss of ZnO-coated samples with the number of ALD cycles is not clearly observed in the results, it might be attributed to the extremely small weight change. It is also necessary to consider the anisotropy of the textured microstructure of the extrudates to understand the role of the ALD ZnO layers. Following post-annealing of the uncoated $Bi_2Te_{2.7}Te_{0.3}$, more pores can be observed in the fracture surfaces perpendicular to the extrusion direction compared to the

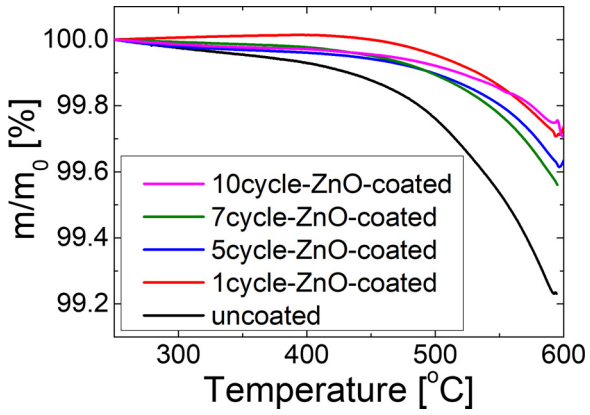

Fig. 4. TGA data for 0, 1, 5, 7, and 10-cycle-ZnO-coated $Bi_2Te_{2.7}Se_{0.3}$ extrudates.

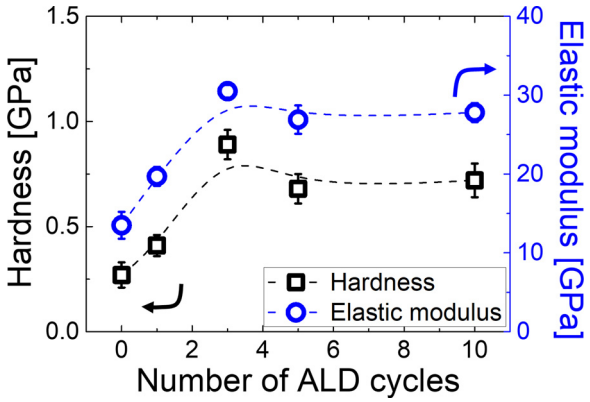

Fig. 6. Variations in the hardness and elastic modulus values of post-annealed extrudates as a function of the number of ALD cycles.

fracture surface parallel to the extrusion direction, with which the basal plane is well aligned (Fig. 5 (a) and (b)). This can be attributed to the anisotropic sublimation behaviour of Bi_2Te_3-based alloys, where Te is predominantly sublimated from non-basal planes [27]. Given that the ZnO layers in the annealed extrudates are generally aligned along the extrusion direction, as shown in Fig. 2 (a), this microstructure arrangement is more effective for the passivation of planes that are susceptible to the sublimation of Te, leading to the formation of relatively dense fracture surfaces (Figs. 3(b) and 5 (c) and (d)).

Another point of interest is that an ALD coating of ZnO on $Bi_2Te_{2.7}Se_{0.3}$ significantly suppresses grain growth during high-temperature annealing. Large grains (> 20 μm) can be observed in the fracture surfaces of the annealed extrudates of uncoated $Bi_2Te_{2.7}Se_{0.3}$ in Fig. 5 (a) and (b). In contrast, the 7-cycle-ZnO-coated $Bi_2Te_{2.7}Se_{0.3}$ is composed of small grains (only a few micrometres), even after post-annealing (Fig. 5 (c) and (d)). The electron backscatter diffraction

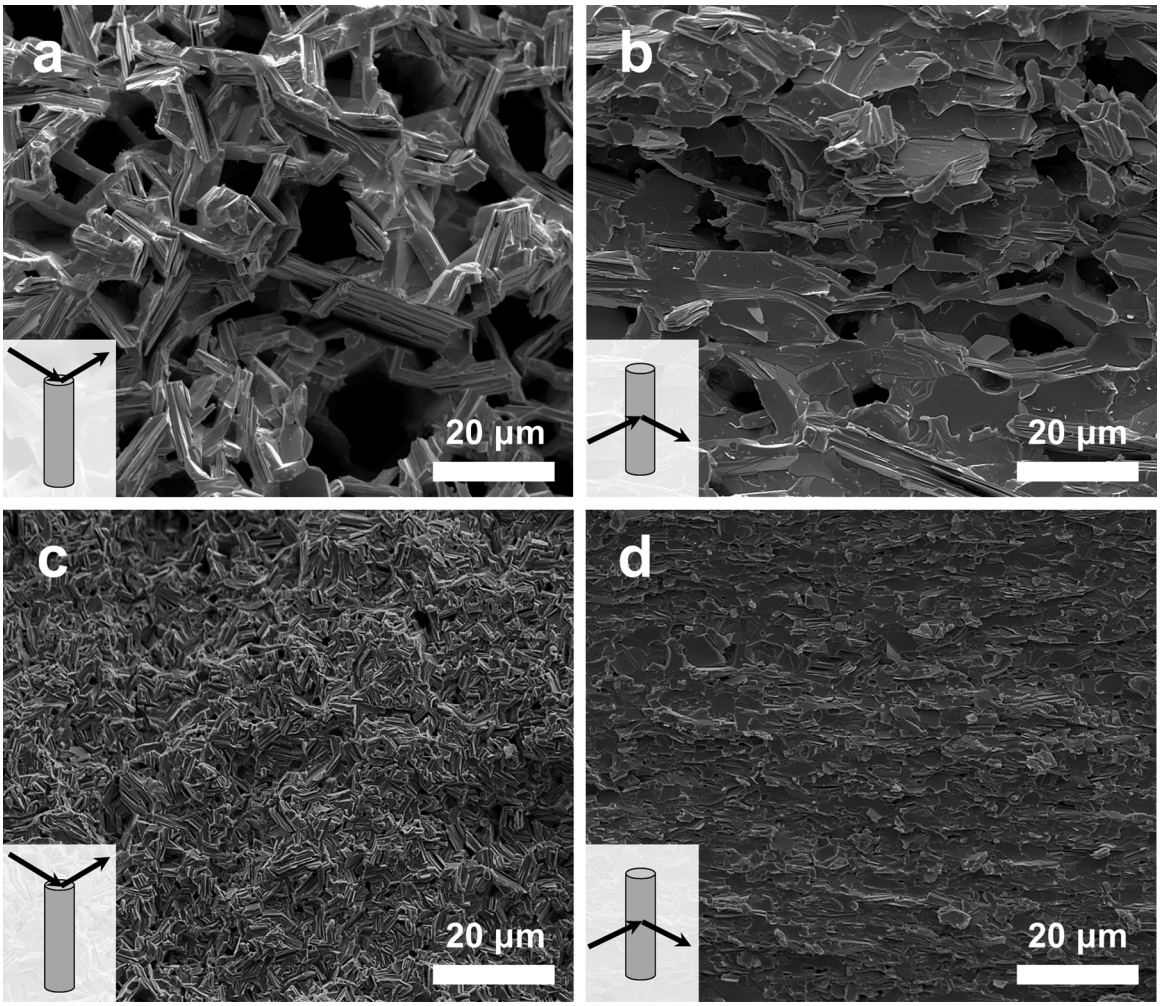

Fig. 5. SEM images of the fracture surfaces of an uncoated $Bi_2Te_{2.7}Se_{0.3}$ extrudate (a) perpendicular to and (b) along the extrusion direction and a 7-cycle-ZnO-coated $Bi_2Te_{2.7}Se_{0.3}$ extrudate (c) perpendicular to and (d) along the extrusion direction.

Table 1
Comparison of the previously reported hardness values of Bi_2Te_3-based alloys.

Materials	Process	Processing Temperature [°C]	Hardness [GPa]	Refs
95 % Bi_2Te_3-5% Bi_2Se_3	Hot extrusion	420	0.58	[28]
Bi_2Te_3-Sb_2Te_3	Equal channel angular extrusion	500	0.60	[29]
Bi_2Te_3	Spark plasma sintering	400	0.80	[30]
25 % Bi_2Te_3-75% Sb_2Te_3	Spark plasma sintering	330	0.65	[31]
95 % Bi_2Te_3-5% Bi_2Se_3	Heat treatment	300	0.45	[32]
95 % Bi_2Te_3-5% Bi_2Se_3	Spark plasma sintering	350	0.57	[33]
Bi_2Te_3	Bridgeman method	585	0.43	[34]
22 % Bi_2Te_3-78% Sb_2Te_3	Spark plasma sintering	N/A	0.60	[35]
20 % Bi_2Te_3-80% Sb_2Te_3	Resistance pressing sintering	490	0.52	[36]

(EBSD) analysis also verified the difference in the grain size. (Fig. S2) This grain growth stagnation is attributed to the uniform dispersion of the thin ZnO layers, which have low movement energy in the $Bi_2Te_{2.7}Se_{0.3}$ matrix. These results suggest that the encapsulation of grains by a thin oxide layer via ALD is a useful method for facilitating grain refinement under severe thermal stress.

The mechanical properties of the samples were examined based on the ALD of a very thin ZnO layer. Fig. 6 presents the variations in the hardness and elastic modulus values of the post-annealed extrudates as a function of the number of ALD cycles. Hardness increases with the number of ALD cycles up to three cycles from 0.27 GPa to 0.75 GPa and becomes saturated above three cycles. For comparison, the reported hardness values of Bi_2Te_3-based alloys were summarized in Table 1 [28–36]. Although the hardness of our uncoated extrudates is much lower than that of the reported values, that of the ZnO-coated extrudates is comparable to or even higher than that of the reported values. The elastic modulus also saturates with an increasing number of ALD cycles from 13 GPa at zero cycles to 30 GPa above three cycles. It should be noted that above three cycles of ZnO ALD, the microstructures appear fully densified (Fig. 3 (b)) and the density of the extrudates becomes saturated (Fig. 3 (d)). This indicates that the mechanical properties of the extrudates are directly related to their microstructures. An ALD coating on $Bi_2Te_{2.7}Te_{0.3}$ powders forms numerous heterogeneous interfaces via grain refinement. As described in the introduction, these interfaces are effective for halting cracks propagation. The low porosity of the ZnO-coated $Bi_2Te_{2.7}Te_{0.3}$ extrudates also contributes to the enhancement of mechanical strength. These results suggest that the ALD coating of grains with very thin ZnO layers significantly improves the mechanical properties of Bi_2Te_3-based alloys, even after harsh thermal treatment.

The thermoelectric properties of the $Bi_2Te_{2.7}Se_{0.3}$ extrudates were also examined in terms of the number of ZnO ALD cycles. Fig. 7 presents the variations in various thermoelectric properties of the $Bi_2Te_{2.7}Se_{0.3}$ extrudates as a function of the number of ZnO ALD cycles. The influence of post-annealing on these properties is also analysed. The σ value of the as-extruded $Bi_2Te_{2.7}Se_{0.3}$ decreases from 2.2×10^5 S/m to 8.4×10^4 S/m as the number of ZnO ALD cycles increases up to seven cycles, then exhibits a slight increase up to 10 ZnO ALD cycles (Fig. 7 (a)). To understand the origin of these changes in the σ, Hall measurements were performed on the samples. The carrier concentration generally decreases with an increasing number of ALD cycles, as shown in Fig. 7 (b), while the Hall mobility of the samples is generally constant, regardless of the number of ZnO ALD cycles (Fig. 7 (c)). The reduction in carrier concentration based on further increase of ZnO cycles may be the result of Zn ions acting as acceptors in $Bi_2Te_{2.7}Se_{0.3}$. It has been reported that some Zn ions from ALD-grown ZnO can diffuse into Bi_2Te_3-based alloys near heterointerfaces, which generates hole carriers based on the substitution of Bi^{3+} with Zn^{2+} [16,37]. Post-annealing also significantly decreases the σ values over the entire range of ZnO ALD cycles based on a reduction in carrier concentration (Fig. 7 (a) and (b)). The sublimation of Te during post-annealing results in the creation of Te vacancies, subsequently inducing the generation of antisite defects of Bi_{Te}' and bismuth vacancies [10]. This process can be expressed by the following equation [38]:

$$Bi_2Te_3 = 2Bi_{Te}' + 2V_{Bi}''' + V_{Te}^{\bullet\bullet} + 3/2Te_2\,(g) + 8\,h^{\bullet} \quad (1)$$

according to Eq. (1), hole carriers are generated by post-annealing, meaning the n-type carrier concentration in $Bi_2Te_{2.7}Se_{0.3}$ extrudates will be reduced by the compensation of holes. As shown in Fig. 7 (d), the S value of the as-extruded sample increases from - 134 μV/K for the uncoated sample to - 207 μV/K for the 7-cycle-ZnO-coated sample. The S values of the extrudates generally increase following post-annealing. The post-annealed extrudates also exhibit a maximum S value of - 234 μV/K with seven ZnO ALD cycles, similar to the as-extruded samples. This trend in the S values is consistent with the variations in carrier density shown in Fig. 7 (b) when considering the inverse relationship between S and carrier concentration. The κ values of the extrudates generally decrease with increasing the number of ALD cycles, and also decrease following post-annealing. (Fig. 7 (e)) Such trend in the κ values is mainly attributed to the change in the carrier concentration. It is found that the κ values of lattice contribution are almost identical irrespective of the ALD cycles while the κ values of electronic contribution decrease with the number of the ALD cycles. (Fig. S3) The invariance of κ values of lattice contribution can be understood by the influences of two different features of the pore formation and the insertion of ZnO layer. Both the features contributed to a decrease in the κ values of lattice contribution [16,39]. As increasing the number of ALD cycles, the pore decreased while the ZnO layer was thicker. The compensation effect might be the reason for the invariance κ values of lattice contribution. Overall, ZT values are increased by the ALD of ZnO (Fig. 7 (f)) because the carrier concentration is properly modulated by the ALD coating. Specifically, the ZT value is enhanced by 40 % following post-annealing with only one cycle of ZnO ALD. These results suggest that the proposed approach based on ALD is a useful method for improving both mechanical and thermoelectric properties.

4. Conclusion

We proposed a novel method for improving the thermoelectric and mechanical properties of Bi_2Te_3-based alloys using an ALD technique. The proposed approach facilitates the synthesis of thermoelectric materials consisting of $Bi_2Te_{2.7}Se_{0.3}$ grains encapsulated by very thin ZnO layers. This microstructure effectively suppresses the sublimation of Te from Bi_2Te_3-based alloys, leading to denser materials following high-temperature processing. Additionally, grain refinement can be achieved via encapsulation by thermally stable ZnO thin layers. Dense thermoelectric materials with many ZnO/ $Bi_2Te_{2.7}Se_{0.3}$ heterogeneous interfaces are effective at impeding movement of dislocations or defects. Therefore, the mechanical properties of extrudates, including hardness and elastic modulus, are significantly improved by ALD coating with ZnO. Furthermore, our approach significantly enhances thermoelectric properties, even with only one cycle of ZnO ALD. We believe that our approach provides a simple and effective method for improving not only thermoelectric properties, but also mechanical properties.

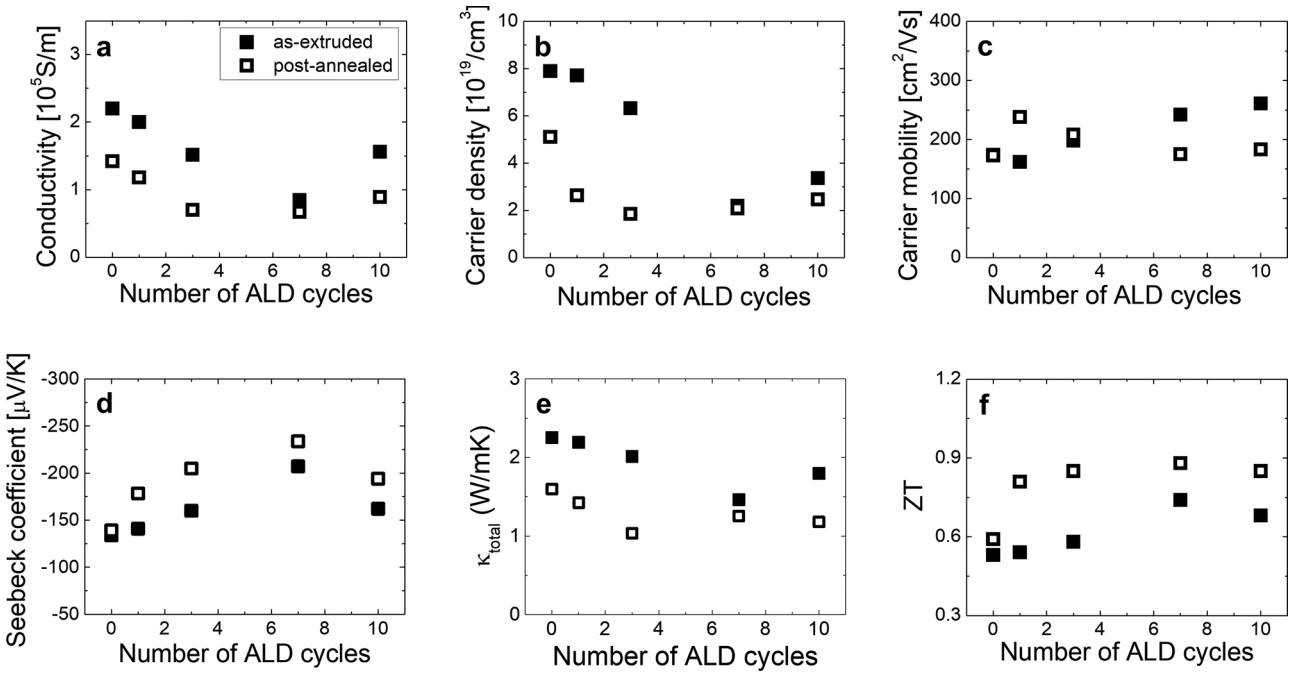

Fig. 7. Thermoelectric properties of the as-extruded and annealed samples as a function of the number of ZnO ALD cycles: (a) electrical conductivity, (b) electron carrier concentration, (c) Hall mobility, (d) Seebeck coefficient, (e) thermal conductivity, and (f) ZT. All measurements were performed at room temperature.

Declaration of Competing Interest

The authors declare that they have no known competing financial interests or personal relationships that could have appeared to influence the work reported in this paper.

Acknowledgements

We would like to acknowledge the financial support from the R&D Convergence Program of NST (National Research Council of Science and Technology) of Republic of Korea. JYK acknowledges the financial support by the fundamental R&D program of Korea Institute of Materials Science (PNK6920)

Appendix A. Supplementary data

Supplementary material related to this article can be found, in the online version, at doi:https://doi.org/10.1016/j.jeurceramsoc.2020.04.013.

References

[1] G.J. Snyder, E.S. Toberer, Complex thermoelectric materials, Nat. Mater. 7 (2008) 105.
[2] F.J. DiSalvo, Thermoelectric cooling and power generation, Science 285 (5428) (1999) 703–706.
[3] J.P. Heremans, B. Wiendlocha, A.M. Chamoire, Resonant levels in bulk thermoelectric semiconductors, Energy Environ. Sci. 5 (2) (2012) 5510–5530.
[4] W. Liu, X. Yan, G. Chen, Z. Ren, Recent advances in thermoelectric nanocomposites, Nano Energy 1 (1) (2012) 42–56.
[5] S.I. Kim, K.H. Lee, H.A. Mun, H.S. Kim, S.W. Hwang, J.W. Roh, D.J. Yang, W.H. Shin, X.S. Li, Y.H. Lee, G.J. Snyder, S.W. Kim, Dense dislocation arrays embedded in grain boundaries for high-performance bulk thermoelectrics, Science 348 (6230) (2015) 109–114.
[6] K.C. Kim, B. Kwon, H.J. Kim, S.H. Baek, C. Park, S.K. Kim, J.S. Kim, Thermoelectric properties of Sn-Doped $Bi_{0.4}Sb_{1.6}Te_3$ thin films, J. Electron. Mater. 44 (6) (2015) 1573–1578.
[7] S.-J. Jung, S.-Y. Park, B.K. Kim, B. Kwon, S.K. Kim, H.-H. Park, D.-I. Kim, J.-Y. Kim, D.-B. Hyun, J.-S. Kim, S.-H. Baek, Hardening of Bi–Te based alloys by dispersing B_4C nanoparticles, Acta Mater. 97 (2015) 68–74.
[8] Y. Pan, T.-R. Wei, Q. Cao, J.-F. Li, Mechanically enhanced p- and n-type Bi_2Te_3-based thermoelectric materials reprocessed from commercial ingots by ball milling and spark plasma sintering, Mater. Sci. Eng. B 197 (2015) 75–81.
[9] Z.J. Xu, L.P. Hu, P.J. Ying, X.B. Zhao, T.J. Zhu, Enhanced thermoelectric and mechanical properties of zone melted p-type $(Bi,Sb)_2Te_3$ thermoelectric materials by hot deformation, Acta Mater. 84 (2015) 385–392.
[10] L.D. Zhao, B.P. Zhang, W.S. Liu, H.L. Zhang, J.F. Li, Effects of annealing on electrical properties of n-type Bi_2Te_3 fabricated by mechanical alloying and spark plasma sintering, J. Alloys. Compd. 467 (1) (2009) 91–97.
[11] T. Hamachiyo, M. Ashida, K. Hasezaki, Thermal conductivity of $Bi_{0.5}Sb_{1.5}Te_3$ affected by grain size and pores, J. Electron. Mater. 38 (7) (2009) 1048–1051.
[12] W. Brostow, T. Datashvili, H.E. Hagg Lobland, T. Hilbig, L. Su, C. Vinado, J. White, Bismuth telluride-based thermoelectric materials: coatings as protection against thermal cycling effects, J. Mater. Res. 27 (22) (2012) 2930–2936.
[13] W. Brostow, I.K. Chen, J.B. White, Effects of polymeric coatings on the service life of bismuth telluride-based thermoelectric materials, Sustain. Energy Fuels 1 (6) (2017) 1376–1380.
[14] Y.I. Shtern, N.V. Igumnova, A.A. Sherchenkov, M.S. Rogachev, M.Y. Shtern, The protective coatings for the multisectional thermoelements of the generators working at the temperatures up to 1200 K, J. Phys. Conf. 857 (2017) 012041.
[15] Y. Zheng, G. Tan, Y. Luo, X. Su, Y. Yan, X. Tang, Thermal Stability of P-Type BiSbTe Alloys Prepared by Melt Spinning and Rapid Sintering, Materials 10 (6) (2017) 617.
[16] K.-C. Kim, S.-S. Lim, S.H. Lee, J. Hong, D.-Y. Cho, A.Y. Mohamed, C.M. Koo, S.-H. Baek, J.-S. Kim, S.K. Kim, Precision interface engineering of an atomic layer in bulk Bi_2Te_3 alloys for high thermoelectric performance, ACS Nano 13 (6) (2019) 7146–7154.
[17] M.-S. Kang, I.-J. Roh, Y.G. Lee, S.-H. Baek, S.K. Kim, B.-K. Ju, D.-B. Hyun, J.-S. Kim, B. Kwon, Correction of the electrical and thermal extrinsic effects in thermoelectric measurements by the harman method, Sci. Rep.-UK 6 (1) (2016) 26507.
[18] I.-J. Roh, Y.G. Lee, M.-S. Kang, J.-U. Lee, S.-H. Baek, S.K. Kim, B.-K. Ju, D.-B. Hyun, J.-S. Kim, B. Kwon, Harman measurements for thermoelectric materials and modules under non-adiabatic conditions, Sci. Rep.-UK 6 (2016) 39131.
[19] B. Min, S.-S. Lim, S.-J. Jung, G. Kim, B.-H. Lee, S.O. Won, S.K. Kim, J.-S. Rhyee, J.-S. Kim, S.-H. Baek, Texture-induced reduction in electrical resistivity of p-type $(Bi,Sb)_2Te_3$ by a hot extrusion, J. Alloy Compd. 764 (2018) 261–266.
[20] S.-J. Jung, B.-H. Lee, B.K. Kim, S.-S. Lim, S.K. Kim, D.-I. Kim, S.O. Won, H.-H. Park, J.-S. Kim, S.-H. Baek, Impurity-free, mechanical doping for the reproducible fabrication of the reliable n-type Bi_2Te_3-based thermoelectric alloys, Acta Mater. 150 (2018) 153–160.
[21] T. Zhu, L. Hu, X. Zhao, J. He, New insights into intrinsic point defects in V_2VI_3 thermoelectric materials, Adv. Sci. 3 (7) (2016) 1600004.
[22] J.M. Schultz, J.P. McHugh, W.A. Tiller, Effects of heavy deformation and annealing on the electrical properties of Bi_2Te_3, J. Appl. Phys. 33 (8) (1962) 2443–2450.
[23] O. Yamashita, S. Tomiyoshi, Effect of annealing on thermoelectric properties of bismuth telluride compounds, J. Appl. Phys. 42 (Part 1, No. 2A) (2003) 492–500.
[24] Z.-L. Wang, T. Araki, T. Onda, Z.-C. Chen, Effect of annealing on microstructure and thermoelectric properties of hot-extruded Bi–Sb–Te bulk materials, J. Mater. Sci. 53 (12) (2018) 9117–9130.
[25] K. Singkaselit, A. Sakulkalavek, R. Sakdanuphab, Effects of annealing temperature on the structural, mechanical and electrical properties of flexible bismuth telluride thin films prepared by high-pressure RF magnetron sputtering, Adv. Nat. Sci: Nanosci. Nanotechnol. 8 (3) (2017) 035002.
[26] G.S.S. Nolas, J. Goldsmid, Thermoelectrics: Basic Principles and New Materials

Developments, Springer, New York, 2001.
[27] J. Buha, R. Gaspari, A.E. Del Rio Castillo, F. Bonaccorso, L. Manna, Thermal stability and anisotropic sublimation of two-dimensional colloidal Bi_2Te_3 and Bi_2Se_3 nanocrystals, Nano Lett. 16 (7) (2016) 4217–4223.
[28] S.-J. Hong, B.-S. Chun, Microstructure and thermoelectric properties of n-type 95% Bi2Te3–5% Bi2Se3 alloy produced by rapid solidification and hot extrusion, Mater. Res. Bull. 38 (4) (2003) 599–608.
[29] J.-T. Im, K.T. Hartwig, J. Sharp, Microstructural refinement of cast p-type Bi2Te3–Sb2Te3 by equal channel angular extrusion, Acta Mater. 52 (1) (2004) 49–55.
[30] L.-D. Zhao, B.-P. Zhang, J.-F. Li, M. Zhou, W.-S. Liu, J. Liu, Thermoelectric and mechanical properties of nano-SiC-dispersed Bi2Te3 fabricated by mechanical alloying and spark plasma sintering, J. Alloys. Compd. 455 (1–2) (2008) 259–264.
[31] C. Moon, S. Shin, D. Kim, T.-S. Kim, Microstructure and thermoelectric properties of p-type Bi2Te3–Sb2Te3 alloys produced by rapid solidification and spark plasma sintering, J. Alloys. Compd. 504 (2010) S504–S507.
[32] M.H. Bhuiyan, T.-S. Kim, J.M. Koo, S.-J. Hong, Microstructural behavior of the heat treated n-type 95% Bi2Te3–5% Bi2Se3 gas atomized thermoelectric powders, J. Alloys. Compd. 509 (5) (2011) 1722–1728.
[33] H.-S. Kim, S.-J. Hong, Thermoelectric properties of n-type 95% Bi2Te3–5% Bi2Se3 compounds fabricated by gas-atomization and spark plasma sintering, J. Alloys. Compd. 586 (2014) S428–S431.
[34] A. Krishna, N. Vijayan, B. Singh, K. Thukral, K. Maurya, Crystalline perfection and mechanical investigations on vertical Bridgman grown Bismuth telluride (Bi2Te3) single crystals for thermoelectric applications, Mater. Sci. Eng. A 657 (2016) 33–37.
[35] C. Jiang, B. Feng, J. Hu, Q. Xiang, G. Li, Y. Li, Z. He, Thermal stability of p-type polycrystalline Bi2Te3-based bulks for the application on thermoelectric power generation, J. Alloy Compd. 692 (2017) 885–891.
[36] J. Hu, C. Jiang, B. Feng, Q. Xiang, G. Li, Z. He, Y. Li, Introduction of porous structure: a feasible and promising method for improving thermoelectric performance of Bi2Te3 based bulks, J. Mater. Sci. Technol. 34 (12) (2018) 2458–2463.
[37] K.C. Kim, C.J. Cho, J. Lee, H.J. Kim, D.S. Jeong, S.H. Baek, J.S. Kim, S.K. Kim, Enhancement of Initial Growth of ZnO Films on Layer-Structured Bi_2Te_3 by Atomic Layer Deposition, Chem. Mater. 26 (22) (2014) 6448–6453.
[38] Z. Starý, J. Horák, M. Stordeur, M. Stölzer, Antisite defects in $Sb_{2-x}Bi_xTe_3$ mixed crystals, J. Phys. Chem. Solids 49 (1) (1988) 29–34.
[39] Y. Wang, W.-D. Liu, H. Gao, L.-J. Wang, M. Li, X.-L. Shi, M. Hong, H. Wang, J. Zou, Z.-G. Chen, High porosity in nanostructured n-Type Bi2Te3 obtaining ultralow lattice thermal conductivity, ACS Appl. Mater. Inter. 11 (34) (2019) 31237–31244.